Applied Catalysis B: Environmental 218 (2017) 91–100

Contents lists available at ScienceDirect

Applied Catalysis B: Environmental

journal homepage: www.elsevier.com/locate/apcatb

Synthesis of Pt+SnO_2/C electrocatalysts containing Pt nanoparticles with preferential (100) orientation for direct ethanol fuel cell

R.M. Antoniassi, J.C.M. Silva, A. Oliveira Neto, E.V. Spinacé *

Instituto de Pesquisas Energéticas e Nucleares – IPEN-CNEN/SP, Av. Prof. Lineu Prestes, 2242, Cidade Universitária, 05508-900 São Paulo, SP, Brazil

ARTICLE INFO

Article history:
Received 29 November 2016
Received in revised form 7 June 2017
Accepted 12 June 2017
Available online 13 June 2017

Keywords:
Pt + SnO2/C electrocatalyst
Preferential (100) orientation
KBr
Fuel cell
DEFC

ABSTRACT

The synthesis of Pt + SnO_2/C electrocatalyst containing cubic Pt nanoparticles with preferential (100) orientation was performed by an alcohol-reduction process using KBr as a shape directing agent. The order of addition of the Pt and Sn precursors and KBr was crucial to obtain cubic Pt particles and a SnO_2 phase with small particle sizes highly dispersed on the carbon support. Electrochemical and DEFC experiments showed that Pt + SnO_2/C electrocatalyst containing Pt nanoparticles with preferential (100) orientation provided superior activity for EOR, power densities and CO_2 selectivity compared to Pt + SnO_2/C electrocatalyst containing Pt polycrystalline.

1. Introduction

New interests related to clean energy generators have been arisen during the past decades due to continuous increasing of fossil fuel consumption and environmental concerns about the global warming. Fuel cell emerged as a technological promise device to supply automobiles, portable and stationary applications, in virtue of being an environmental-friendly electrochemical machine, robust, noise-free and efficient energy supplier when active catalysts are used on their both electrodes. Among various types of fuel cells, Proton Exchange Membrane Fuel Cell – *PEMFC* has attracted a particular attention because of its direct potential application in vehicles to replace the current internal combustion engines. Hydrogen is the principal combustible used in PEMFCs, which is oxidized on anode electrode while oxygen, usually from air, is reduced on cathode side. Although only water and heat are produced at the final reaction, and thereby PEMFCs are considered a clean energy generator, hydrogen is still mainly obtained by steam hydrocarbons reforming, which produces an impure combustible (must be purified before using it) or by a high cost water electrolysis process. In this sense, PEMFC is flexible to work with other combustibles such as methanol [1] and ethanol [2,3] without any structural modification. Direct Ethanol Fuel Cell – *DEFC* presents some technical advantages regarding to ethanol production and manipulation, since it comes from cheap and renewable sources and it can be easily stored in liquid tanks. However, finding electrocatalysts that promote the C—C bond cleavage efficiently remainsthe main challenge. When ethanol molecule is not completely oxidized to CO_2, acetaldehyde and acetic acid are produced, and DEFC losespart of its high efficiency. Moreover, some incompletely ethanol electro-oxidation fragmentssuch as carbon monoxide and methyl groups may poison catalyst surface, leading to a cell performance loss over time [2].

Dealing with catalyst field, platinum (and Pt-based) nanostructures are considered as the principal metal for innumerous applications such as environmental reactions towards reduction of air pollutants, medicine, photonics and electrocatalysts of the fuel cells itself [1–7]. Recently, continuous efforts devoted on size, composition and even morphology modifications have been conducted on the use of Pt nanoparticles in various reactions in order to enhance the catalytic activity. Through a rational design of synthesis, it is possible to achieve materials with particular characteristics, thus tuning their catalytic performance [7]. Morphological changes on metal nanoparticles are no longer an artwork but it became a science issue, since researchers are already capable to catch up the opportunities that nanosized materials can offer.

Different geometries are achieved by an appropriated atomic arrangement, that is to say, by controlling the exposition of crystallographic facets. All noble metals naturally crystallize in face-centered cubic structure (FCC). Following thermodynamics predictions, the energy surface energy increases according to the direction g{111} < g{110} < g{100}, which results in a truncated

* Corresponding author.
E-mail addresses: espinace@ipen.br, espinace@yahoo.com.br (E.V. Spinacé).

http://dx.doi.org/10.1016/j.apcatb.2017.06.031
0926-3373/

octahedral crystallization. If this thermodynamic growth regime is, somehow, modified by chemical agents or by electrochemical approaches, nanoparticles can assume different morphologies. Some reports of Pt nanoparticles produced in various geometries such as cubes [8], cuboctahedral [9], octahedral [10], wire [11], tetrahedral [12], branched [13] are found in literature. Most of them were prepared by chemical methods, which are more suitable in terms of providing a greater control of size and morphology of the nanoparticles. Since El-Sayed's group [10] firstly reported colloidal Pt with different morphologies by using capping agents (sodium polyacrylate), the employment of stabilizing agents had become prevalent in faceted material synthesis. Agents like polyacrylate, polyvinylpyrrolidone (PVP), oleylamine are important in synthesis of colloidal shaped nanoparticles, preventing overgrowth and agglomeration of the nanoparticles as well as allowing a better size control of the resulted material. The application of these materials on fuel cells, however, requires a previous step of cleanness, since such organic compounds largely block metal active sites. Many severe cleaning methods to remove stabilizing agents including thermal treatment [14], ultraviolet radiation [15], strong oxidizing compounds, like H_2O_2/H_2SO_4 solution [16] or organic solvents [17] might lead to an aggregation and/or destruction of the nanoparticles [18], making this approach nonviable for scale-up purposes. Subsequently, a separated step of deposition would be needed to anchor nanoparticles on a support surface (usually on carbon), even involving anchoring agents. Kim et al. [19] synthesized Pt nanocubes directly nucleated and overgrown on carbon support by using cysteamine to conduct the particles deposition. Aiming fuel cell applications and considering the large scale possibility, it is fundamental to proceed with a synthesis as simple as possible, by preparing materials via unique reduction/anchoring step, using fewer reagents and free of organic impurities. Studies on Pt or Pt-based catalysts directly reduced and anchored on carbon support are scarce in the literature, especially for fuel cells [20], indicating that producing and applying such special materials is not a trivial deal.

Considering monocrystals or unsupported faceted materials with desired morphologies, Feliu and co-workers [21] produced unsupported cubic Pt(100) preferential particles by a water-oil reduction method using H_2SO_4 and HCl as surface modifiers. Their material exhibited a good activity for CO and ammonia electro-oxidations, which are surface structure sensitive reactions. In another publication, they anchored these Pt nanoparticles on carbon support and tested for ammonia and formic acid electro-oxidations [22]. Figueiredo et al. [20] also synthesized Pt(100) preferentially oriented particles by the same water in oil method and supported in carbon. The authors claimed that the observed enhanced ethanol electro-oxidation activity might be consequence of C—C bond breaking on the selective sites. Han and collaborators [8] synthesized Pt(100) nanocubes controlled by PVP and Fe^{+3} additions and showed the importance of the surface toward methanol and ethanol electro-oxidation activities. Single crystals can be used as a model to predict activity of preferential oriented nanoparticles. Through cyclic voltammetry and FTIR technique, Busó-Rogero[23] revealed activity and selectivity towards ethanol electro-oxidation being readily affected by surface arrangement. In this occasion, they showed that acetic acid is major produced in Pt(111) particles domains, and CO_2 quantities is neglible, while rich-(100) Pt nanoparticles can break C—C bond easier. As mentioned above, ethanol electro-oxidation activity and its products selectivity can be driven by tailoring Pt facets. In a recent paper, we have demonstrated that cubic preferentially oriented Pt(100), directly supported on Carbon Vulcan, can be prepared via single step, without any stabilizing or anchoring compounds, only using bromine ions as shape directing agent [24]. The control of addition of the Pt precursor and KBr was crucial to achieve supported cubic Pt with units of nanometer. Bromine ions were employed to adsorb on metal surface, thus leading to an anisotropic growth of platinum nanoparticles; the significance of this approach was to state that a simple water washing process completely removed all adsorbed anions. The resulted material provided superior power density and CO_2 selectivity in DEFC tests compared to polycrystalline Pt/C [24]. However, it is known that a second element combined to platinum can make the electrocatalyst more tolerant to carbonaceous poisons, thus enhancing the ethanol electro-oxidation reaction (EOR) activity. The combination of Pt and Sn supported in carbon is the most promising material for DEFC, providing high current densities [25]. Herein we report a simple strategy to synthesize $Pt + SnO_2/C$ electrocatalyst containing cubic Pt nanoparticles with preferential (100) orientation directly supported on carbon, employing only KBr as a shape directing agent. Some synthesis procedures and real DEFC electrical performance are discussed.

2. Experimental

2.1. Preparation of PtSn electrocatalyst containing Pt nanoparticles with preferential (100) orientation directly on the carbon support (Pt+SnO_2/C electrocatalysts)

The following materials were used to produce $Pt + SnO_2/C$ electrocatalyst: hydrated hexacloroplatinum (IV) acid ($H_2PtCl_6{\cdot}6H_2O$, 99.95% purity) and hydrated tin (II) chloride ($SnCl_2{\cdot}xH_2O$, 99,99%) as metal sources (3Pt: 1Sn atomic ratio), potassium bromide (KBr, 99.7%), Vulcan Carbon (X72R – Cabot Corporation), ultrapure water and ethylene glycol (EG). $Pt + SnO_2/C$ (20 wt% of metal load) electrocatalysts were synthesized by an alcohol-reduction process [24] by adding $H_2PtCl_6{\cdot}6H_2O$ and KBr into an EG/H_2O 3/1 (v/v) solution. The carbon support was quickly added into this solution, which was sonicated for 5 min. The resulting mixture was kept under reflux at 150 °C for 3 h before being filtered, washed with abundant water and dried for 3 h at 80 °C. The order of addition of $SnCl_2{\cdot}xH_2O$ and KBr was studied.

2.2. Physical-chemical characterizations

Morphology, size and dispersion of $Pt + SnO_2/C$ electrocatalysts were evaluated by transmission electron microscopy (TEM –JEOL model JEM 2100F, operating at 200 kV). For TEM observations, an amount of the electrocatalyst was suspended in isopropyl alcohol and dropped in TEM grid coated with collodion film. The size was measured by end-to-end particle's extension. The catalysts were also investigated by Dark-Field (STEM-DF) technique. The compositional distribution (mapping) was investigated by XEDS in the STEM mode. X-ray dispersive spectroscopy (EDS) coupled to a JEOL JSN 6010LA scanning microscopy, operatingat 20 kV, was employed to verify the elementary Pt and Sn contents. X-ray diffraction (XRD) analyses were carried out by a Rigaku Miniflex II apparatus, using CuKa radiation. The diffracrograms range 2q was between 20–90° with a scan rate of $0.025^\circ\ s^{-1}$.

Using a 910 PSTAT (Metrohm) potentiostat, cyclic voltammetry technique (CV) was employed for surface and electrochemical studies. A three-electrodes cell apparatus with an ultrathin vitreous carbon layer previously polished was used as work electrode, a platinum plate as counter electrode and hydrogen electrode (RHE) as reference. An aliquot of sonicated catalytic ink containing water (0.9 mL), isopropyl alcohol (0.1 mL), Nafion® solution (5%) (0.02 mL) and the catalytic powder (1 mg) was dropped on the tip of work electrode. For its preparation, it was deposited 2 mg of Pt equivalent content on the carbon vitreous layer and let air dried. Sulfuric acid ($0.5\ mol\ L^{-1}$) was employed as support electrolyte. After nitrogen gas was bubbled into H_2SO_4 solution for 30 min, CVs were

recorded at a scan rate of 50 mV s^{-1} at ambient temperature. Subsequently, ethanol oxidation reaction experiments were conducted with 20 mmol L^{-1} of ethanol solution. For CO-stripping experiment, the work electrode was polarized at 0.25 V and carbon monoxide was bubbled during 15 min into electrolyte, followed by nitrogen gas for 30 min. For normalization purposes, CO electroactive area was calculated, following the Eq. (1) below:

$$ESCA_{CO} = \frac{Q_{CO}}{[Pt]\, q^0_{CO}} \quad (1)$$

where Q_{CO} is the CO oxidation charge, considering the electrical double layer contribution; [*Pt*] is the platinum loading and q^0_{CO} is the charge required to oxidize a CO monolayer adsorbed over platinum (420 mC cm^{-2}).

2.3. Single DEFC electrical performance

For MEAs (Membrane Electrode Assembly) preparation, synthesized Pt + SnO_2/C were evaluated as anodes while commercial Pt/C (BASF, lot# F0381022) was chosen as cathode. Both 5 cm^2 electrodes (containing 1 mg_{Pt} per cm^2) were hot pressed to a pretreated Nafion 115 membrane (Dupont) electrolyte at 125 °C for 10 min. All prepared MEAs were inserted in a single cell, operating at 100 °C, fueled with 2 mL min^{-1} of ethanol (2 mol L^{-1}) and 500 mL min^{-1} of oxygen at 2 bar. The actual electrical performance of the electrocatalysts was evaluated by polarization and power density curves, normalized per electrode geometric area.

2.4. Products distribution by gas chromatography

The reaction of ethanol electro-oxidation products were determined and quantified by gas chromatography technique by using a gas chromatograph (GC), model Agilent 7890 A. In these experiments a capillary column Plot-U (30 m) and a thermal conductivity detector (TCD) were employed. The elution gas was carried out using hydrogen gas with a flow rate of 45 mL min^{-1} and the oven temperature was maintained at 80 °C for 5 min and, afterwards, it was increased at 10 °C min^{-1} until reach 160 °C. Inlet and detector temperatures were set to 180 °C and 220 °C, respectively. Aliquots (collected over the condition at maximum power density and at a constant value of 0.1 A cm^2 current density) of the single cell anodic effluent was cooled in an ice bath before to be manually injected into GC.

3. Results and discussion

Initially, we observed the influence of adding Sn precursor at different synthesis stages on the nanoparticles morphology. Following our successfully methodology to obtain Pt cubic shaped nanoparticles [24], Pt + SnO_2/C 30.70 syntheses were performed by adding 30 wt% of Pt precursor into an EG/H_2O solution containing Carbon Vulcan support and the reaction was allowed to proceed for 15 min until KBr addition. After 20 min of KBr addition the remainder 70 wt% Pt precursor was quickly added. Sn precursor was added at different synthesis stages (marked by I, II or III), as shown in Fig. 1. For a comparison purpose, Pt + SnO_2/C (Fig. 1**a**) was prepared without the addition of KBr, through one step Pt and Sn precursors addition. In this case, the obtained Pt + SnO_2/C electrocatalyst exhibited spherical shaped nanoparticles, well-dispersed on the carbon support with size of about 3 nm (see Table 1). Fig. 1**b** shows Pt + SnO_2/C 30.70 I micrograph, in which 30 wt% of Pt precursor and the total amount of Sn precursor were added at the beginning of the synthesis. After 15 min under reflux KBr was added, followed by the remainder 70 wt% of Pt precursor, as already described on Pt/C electrocatalyst with (100) preferential orientation synthesis [24].

Table 1
Physical-chemical characterizations: particle size, facet domain and atomic composition of the prepared materials.

Electrocatalyst	TEM particles size (nm)	$XRD_{(111)/(200)}$ ratio	Pt: Sn atomic ratio
Pt + SnO_2/C	3.2 ± 0.6	2.31	71:29
Pt + SnO_2/C 30.70 I	7.7 ± 3.6	1.96	74:26
Pt + SnO_2/C 30.70 II	5.9 ± 0.7	1.70	72:28
Pt + SnO_2/C 30.70 III	7.8 ± 1.6	1.42	72:28

The micrograph showed that the nanoparticles were not in cubic geometry. Besides, an agglomeration phenomena was observed, suggesting that Sn interferes, somehow, on the growth mechanism in such conditions. When Sn was shortly added after the 70 wt% of remaining Pt precursor (Pt + SnO_2/C 30.70 II in Fig. 1**c**) and the system remained under reflux for a long time of reaction (90 min), 6 nm spherical shaped particles were observed. Cubic shaped nanoparticles were exclusively achieved if the Sn precursor is added at the final step of the synthesis (Pt + SnO_2/C 30.70 III in Fig. 1**d**), that is, if the system remains under reflux for a short time of reaction (10 min) after the addition of Sn precursor. Despite the fact that their mean size was more than twice bigger than the material without KBr, nanoparticles were relatively well-dispersed on carbon support, such discoveries were also observed for cubic Pt/C [24]. Thus, from TEM analyses, one could note that Sn precursor addition directly modifies the nanoparticles morphology and dispersion. Similar results can be observed from XRD measurements. From Table 1 it is possible to note that the (111)/(200) peak intensity ratio decreased in the following order: Pt + SnO_2/C 30.70 III > Pt + SnO_2/C 30.70 II > Pt + SnO_2/C 30.70 I > Pt + SnO_2/C. Pt(100) surface domains were more intense for materials prepared in the presence of KBr and especially for Pt + SnO_2/C 30.70 III, which exhibited more abundant (200) planes, as a result of cubes formation. However, it was possible to check that the Sn precursor also influenced on (111)/(200) peak intensity ratio. This ratio is increased when Sn precursor was added on the beginning of the synthesis (Fig. 1**b**) or if Sn remained for a long time in the synthesis medium (Fig. 1**c**). This fact suggests that Sn precursor can both inhibit the preferential formation Pt(100) domains and lead to the Pt nanoparticles agglomeration (Fig. 1b). EDS analysis showed that all obtained materials have measured atomic Pt:Sn ratios close to the nominal 3:1 value. Bromide signals were not observed in all materials, indicating Pt + SnO_2 nanoparticles were cleaned from KBr shape direct agent (Pt + SnO_2/C 30.70 III). EDS spectrum is shown forward in the text. The choice of Pt:Sn (3:1) molar ratio was based on a previous work [25]. Among others, $Pt_3(SnO_2)$ formulation yielded the greater ethanol conversion in products (in molar units), consequently enhancing the DEFC electrical performance.

In order to investigate the morphological changes of Pt + SnO_2/C 30.70 III nanoparticles, some samples were collected during different synthesis times. Fig. 2 shows TEM observations of temporal evolution of the nanoparticles morphology. From Fig. 2**a**, it was already possible to verify nanoparticles presence past 10 min to the first Pt precursor addition. They appeared spherical shaped, with 3–4 nm and well-dispersed on carbon support. After 10 min from KBr addition (Fig. 2**b**), nanoparticles size almost doubled to 5.5 nm, but spherical geometry remained. Nanoparticles only began to assume cubic morphology after the second Pt precursor addition, i.e., 45 min later the first addition (Fig. 2**c**). At this time, we could check some well-dispersed cubes of 6–7 nm. Through this reducing methodology, it is important to say that nanocubes were only achieved if Pt ions (H_2PtCl_6 precursor) were reduced on the pre-reduced Pt seeds, in KBr presence. Taking into account the nanocubes achieved at 45 min of synthesis, we return to Fig. 1c and by observing spherical shaped nanoparticles, it can be stated that Sn precursor, added over the 90th min, was responsible for

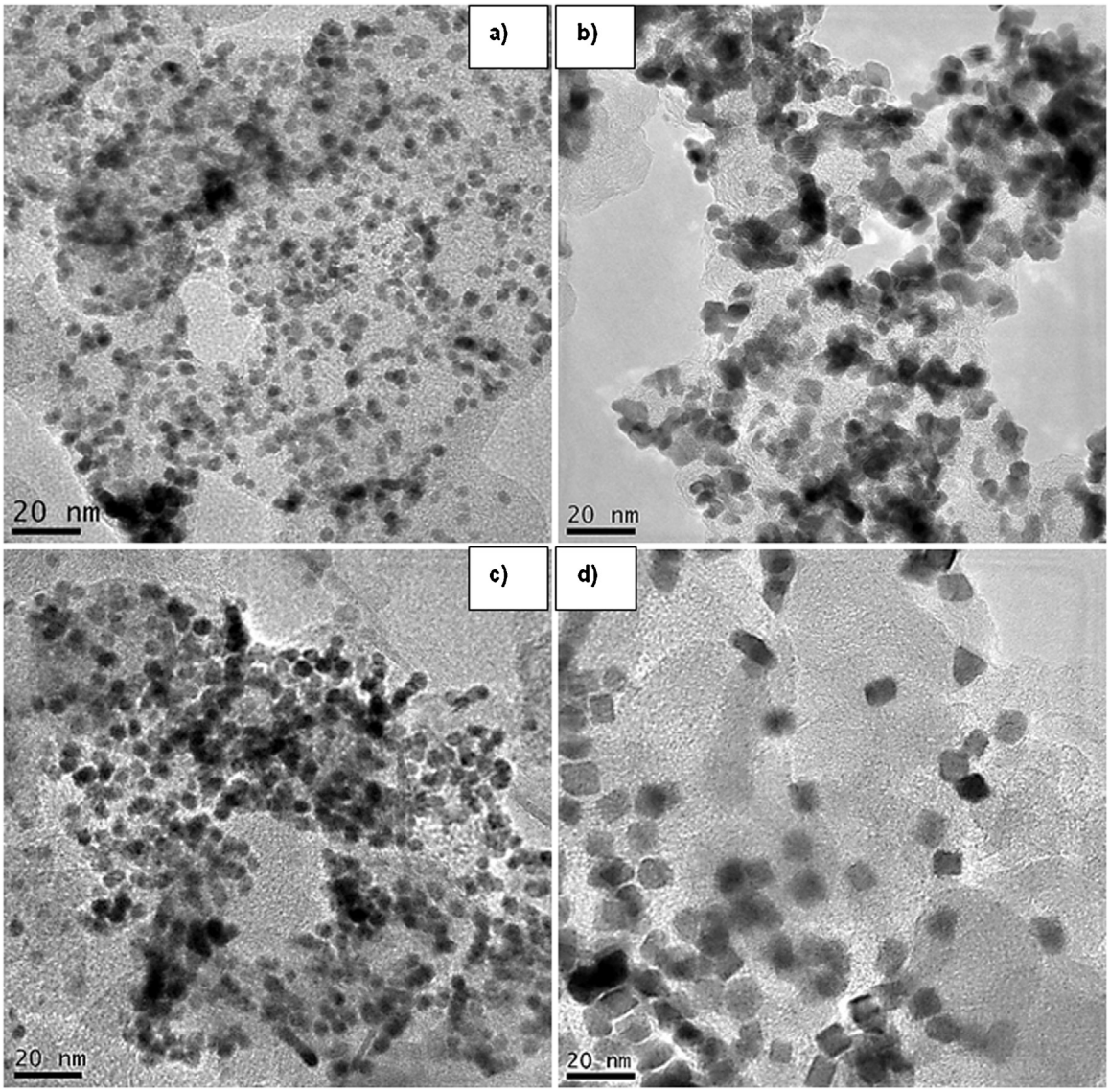

Fig. 1. Influence of Sn precursor addition. TEM of carbon deposited Pt + SnO_2 at the end of 3 h of synthesis. **a)** Pt + SnO_2/C preparing in a single step without KBr addition, **b)** Pt + SnO_2/C 30.70 I with Sn precursor added at the beginning of the synthesis, **c)** Pt + SnO_2/C 30.70 II with Sn precursor added after 90 min and **d)** Pt + SnO_2/C 30.70 III with Sn precursor added 170 min.

degenerating the cubic geometry yielding into 6 nm spheres. Fig. 2**d** shows that all nanocubes are practically built at 10 min before to add Sn precursor. At this time, nanocubes grew up to 8 nm with a good uniformity on carbon support. Finally, adding Sn source at the ending of the synthesis was a key factor to preserve the desired morphology with abundant Pt(200) surface domains. Passed 10 min of Sn precursor addition, it was possible to observe that nanoparticles maintain shape and uniformity on the carbon support (Fig. 2**e**). Moreover, Pt nanoparticles do not change their size after the Sn precursor is added (approximately 8 nm), indicating Pt nanoparticles structure was preserved. This suggests Pt and Sn have structurally independent phases, in other words, Sn precursor exclusively leads the SnO_2 formation, which coexists with Pt nanoparticles. Fig. 2**f** shows a detailed nanocube from Pt + SnO_2/C 30.70 III, where it is possible to check out the atomic lattice fringes. The measurement of the interplanar distance pointed out 1.95 Å, which represents the $d_{(200)}$ enclosed facets that extended until the cubic edge sides, thus confirming the preferential Pt(100) orientation.

Fig. 3 reveals some details about structure and composition of Pt + SnO_2/C 30.70 III catalyst through XRD and STEM analyses. Fig. 3**a** shows the X-ray diffraction data of Pt + SnO_2/C and cubic Pt + SnO_2/C 30.70 III. Both XRD profiles exhibited one peak at approximately 2q = 25°, which represents the carbon Vulcan support, and five more peaks at 39°, 46°, 67°, 81° and 85°, assigned to (111), (200), (220), (311) and (222) of Pt face-centered cubic structure (Pt-FCC) [25]. The different broadening of Pt diffraction peaks was a result of their difference in crystallite size. In this case, greater crystals were found in Pt + SnO_2/C 30.70 III (sharper peaks) compared to Pt + SnO_2/C (broader ones), also confirmed by TEM images. There were two contributions in 2q ≈ 33° and 52° relative to SnO_2 (cassiterite phase). These peaks are broad and have low intensity due to the low crystallinity and/or small particle size [25,26], since EDS analysis confirms the right content of Sn and Pt. Graphical inset zoomed in the SnO_2 small contribution at approximately 33°, which is relative to (101) cassiterite structure. Pt-FCC peaks have no horizontal shift towards minor 2q angles, indicating no Pt-Sn in alloyed arrangement, that is to say, Pt and SnO_2 coexist in the material. Fig. 3**b** exhibits EDS spectrum data of Pt + SnO_2/C 30.70 III, which confirms no bromide contamination on the catalyst composition. From the STEM-DF of Fig. 3**c** it is possible to

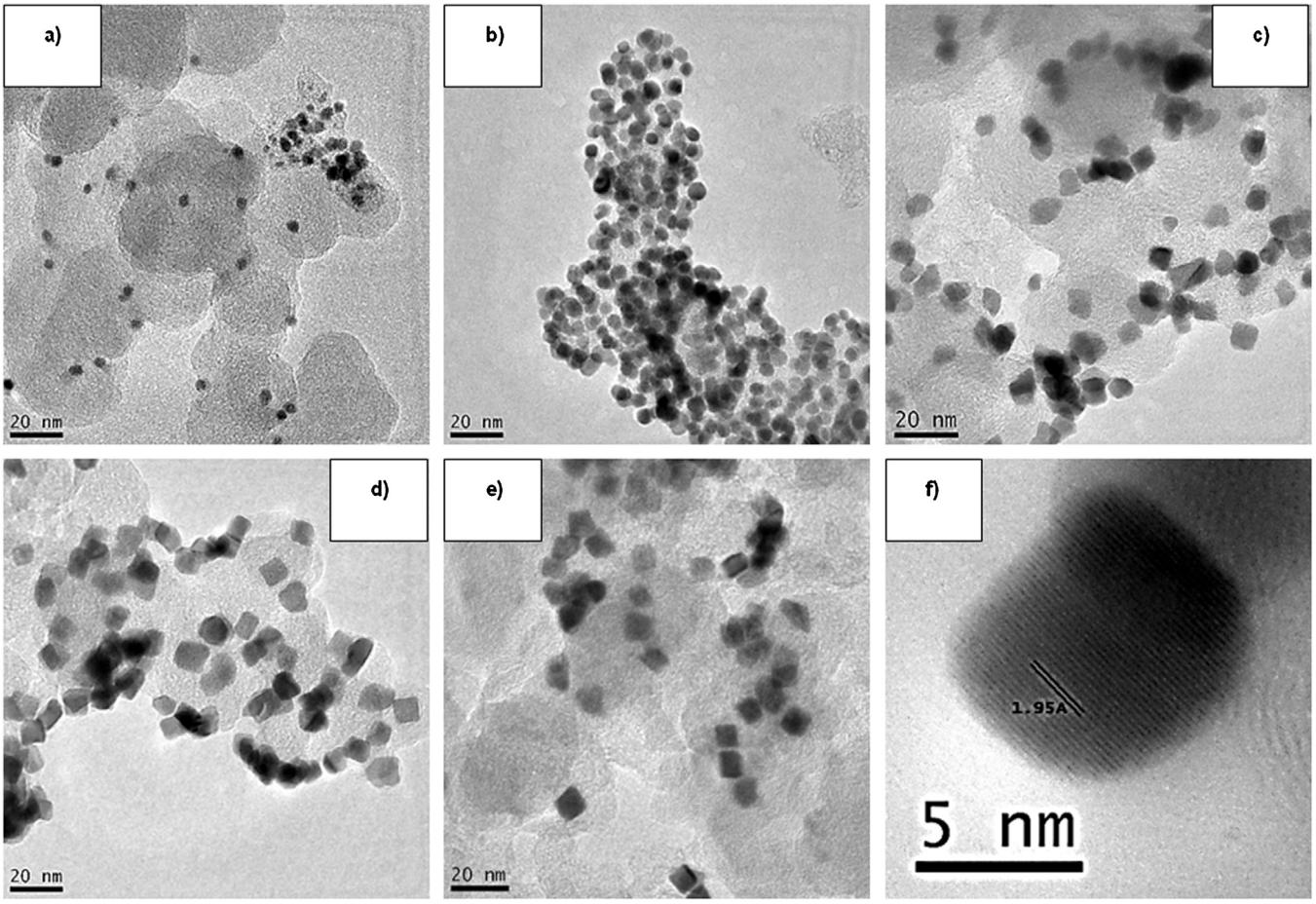

Fig. 2. Temporal Evolution ofthe nanoparticles morphology from Pt + SnO_2/C 30.70 III electrocatalyst (samples collected at different synthesis times), **a)** Pt + SnO_2/C 30.70 III without the KBr addition **b)** Pt + SnO_2/C 30.70 III ten minutes after the KBr addition, **c)** Pt + SnO_2/C 30.70 III ten min after the complementary Pt source addition, **d)** Pt + SnO_2/C 30.70 III ten min before the Sn source addition, **e)** Pt + SnO_2/C 30.70 III after 3 h of synthesis and **f)** detailed cube from e).

observe in the centre of the image two cubic nanoparticles sized about 8 nm. Through mapping the elements by XEDS, it was verified that nanoparticles surface (Fig. 3**d**) contains both platinum (red spots) and tin (green spots) signals. Pt La1 and Sn La1 counts were evidenced in the chosen area by the same colors. A concentrated counting of platinum fits at the exactly position of cubic structures (Fig. 3**e**). However, Sn spots appeared over the entire region, but a greater concentration on the nanoparticles position was observed (white arrows in Fig. 3**f**). This means that nanocubes are mainly composed by Pt, while SnO_2 is uniformly distributed all over the material. Brightness is a function of atomic number in STEM-DF technique (Z-contrast image); brighter areas represent higher average atomic numbers (Pt or Sn particles). Brighter cubic shaped nanoparticles with approximately 8 nm are seen in the STEM-DF image, which are assigned to Pt particles (Fig. 3**g**). However, neither any nanoparticles of SnO_2 surrounding the Pt cubes nor deposited on carbon support could be verified. This fact is in agreement with XRD observations, demonstrating the presence of SnO_2 is in a submicroscopic level. All supported Pt nanocubes are in contact with dispersed SnO_2 homogeneously distributed on the carbon support, however further studies are necessary to confirm this hypothesis.

Materials built by different surface arrangements may present distinct cyclic voltammetry profiles. CV technique was employed to verify the basal Miller planes of the prepared materials through the so-called hydrogen adsorption/desorption region. In order to avoid the destruction of the structural characteristics, CVs were recorded in H_2SO_4 (0.5 mol L^{-1}) electrolyte, at a limited potential range of 0.05–0.8 V. Based on previous investigations related to hydrogen adsorption/desorption on platinum monocrystals surface in acid media [27,28], the peak close 0.125 V (*vs* reference hydrogen electrode – RHE) corresponds to the process on Pt(110) type sites, while those ones at 0.27 and 0.35 – 0.37 V are attributed to step and terrace sites of Pt(100) facets, respectively. In Fig. 4**a** are shown the CVs performed in sulfuric acid at a 50 mV s^{-1}. Observing Pt + SnO_2/C CV, it was not possible to observe a well-defined hydrogen adsorption/desorption region if compared to Pt/C profile [24]. Similar profiles were already verified for polycrystalline PtSn-based catalysts [29,30]. Meanwhile, in Pt + SnO_2/C 30.70 III all the three aforementioned contribution peaks were readily identifiable, probably due to its higher surface orientation. In addition, the (100) contribution at 0.27 V was greater than that (110), such profile is in accordance with achieved Pt and Pt/C nanocubes previously reported [22,24]. Absent in Pt + SnO_2/C CV profile, the Pt(100) terrace domain is evident at 0.35 – 0.37 V in Pt + SnO_2/C 30.70 III, thus confirming again its preferential exposed facet.

Fig. 4**b** presents electro-oxidation of one layer of absorbed carbon monoxide, generally known by CO-stripping. Carbon monoxide has a structural sensitive interaction on Pt sites; therefore, it can be used as a molecular probe to study surface modifications in Pt or Pt-based materials [31]. As can be seen Pt + SnO_2/C and Pt + SnO_2/C 30.70 III exhibited two different CO-stripping profiles. In CO-stripping using Pt + SnO_2/C, only one peak from CO electro-oxidation was observed and its onset potential was about 0.45 V. The same single CO-stripping peak profile was already noticed for PtSn-based materials in [32,33]. Interestingly, there was a peak split in Pt + SnO_2/C 30.70 III profile, and two other peaks can be readily

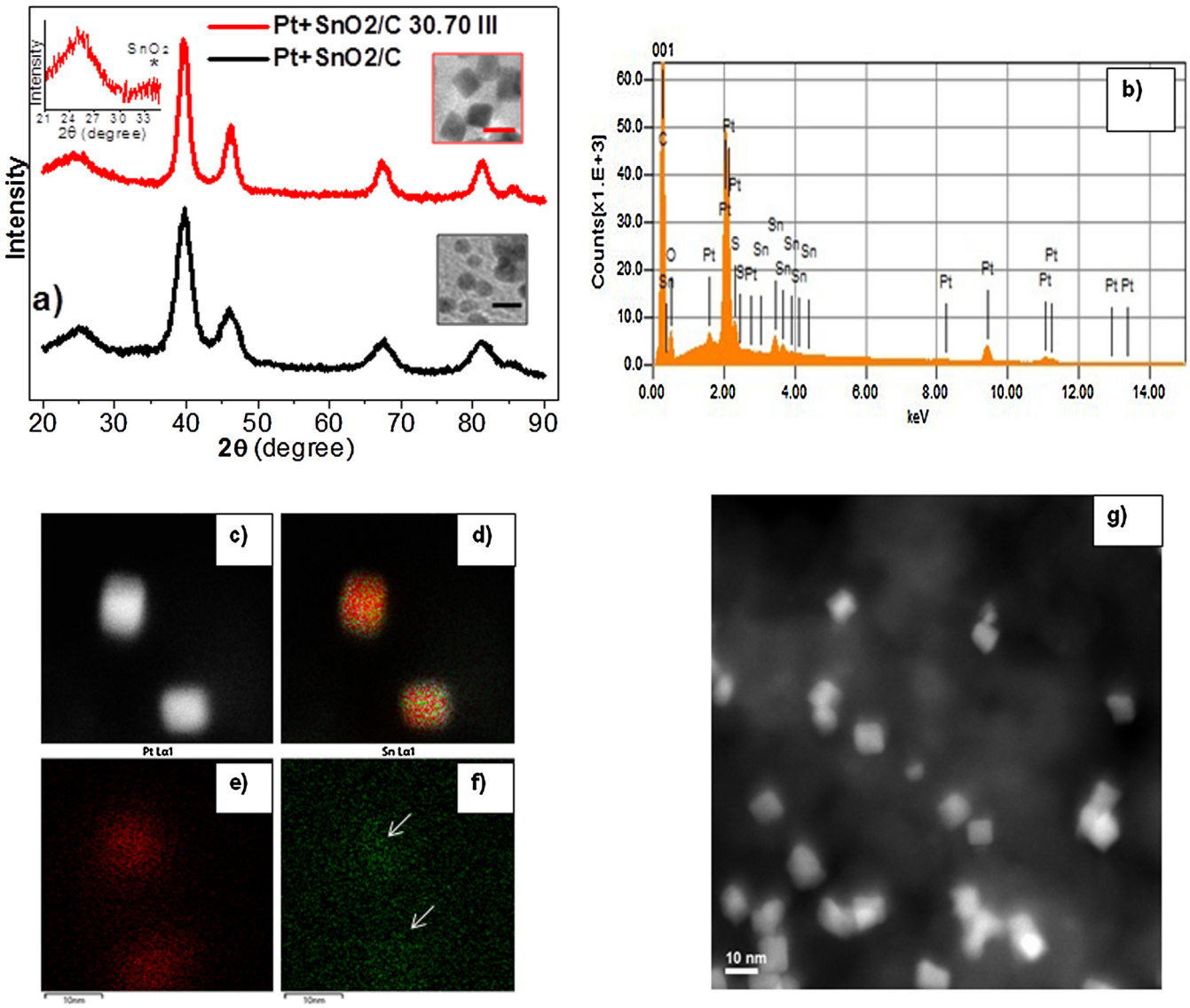

Fig. 3. **a)** X-ray diffraction (TEM image bar 10 nm), **b)** EDS chemical spectra of Pt + SnO_2/C 30.70 III, **c)** STEM-DF image of cubic nanoparticles in Pt + SnO_2/C 30.70 III material, **d)** XEDS chemical mapping on the Pt + SnO_2/C 30.70 III nanoparticles, **e)** and **f)** Pt and Sn mapping of c) and **g)** view of the nanoparticles distribution with STEM-DF technique.

observed at 0.65–0.75 (I) and 0.79 V (II). It is reasonable to expect that modifications on Pt surface promote differences in carbon monoxide adsorption, hence in CO-stripping feature. Some results in literature reported that, depending on the adsorption sites, the CO electro-oxidation can proceed at different potentials values, usually leading a peak splitting [34]. In such occasion, the authors claimed that high potentials are needed to oxidize adsorbed CO near on the edge and/or corners while on terrace surfaces it occurs at lower values. Considering our CO-stripping profile, the peak split might be associated to an increased Pt(100) terrace surface domains contained in cubic Pt + SnO_2/C 30.70 III, rather than in irregular surface of the spherical shaped nanoparticles of Pt + SnO_2/C. According to the literature [35,36], the peak found at 0.65–0.75 V (I) is related to CO electro-oxidation on the long range Pt(100) bi-dimensional surfaces, whereas the peak at 0.79 V (II) might represent the process on short range Pt(100) domains. In addition, a pre-peak (PP) at 0.42 V was also found in Pt + SnO_2/C 30.70 III profile, which is related to a weaker adsorbed CO electro-oxidation. Coutanceau and co-workers [37] performed CO-stripping technique in unsupported cubic Pt(100) nanoparticles and explained the pre-peak in terms of weakly adsorbed CO due to CO—CO lateral repulsive interactions.

Fig. 4**c** shows the voltammetric profiles of ethanol electro-oxidation reaction, normalized in terms of CO electroactive area ($ECSA_{CO}$). Pt + SnO_2/C exhibited an $ECSA_{CO}$ of 1.56 $m^2\ g_{Pt}^{-1}$, value almost 40% greater than that for Pt + SnO_2/C 30.70 III, which is expected considering the catalysts size difference. The onset potential of EOR for Pt + SnO_2/C 30.70 III (~0.45 V) was slightly lower than for Pt + SnO_2/C (~0.50 V). Besides, comparing their forward scan, Pt + SnO_2/C 30.70 III exhibited a maximum current density of 81 A cm^{-2}, value 25% higher than Pt + SnO_2/C. Both current densities were also normalized per platinum load and Pt + SnO_2/C 30.70 III showed superior values again (55 A g_{Pt}^{-1} against 48 A g_{Pt}^{-1} from Pt + SnO_2/C). This indicates that Pt + SnO_2/C 30.70 III has a superior catalytic activity than Pt + SnO_2/C towards EOR. It is well-known that carbonaceous intermediates from EOR (mainly CO) can strongly adsorb and easily block Pt active sites, leading to their fast deactivation. The higher activity obtained by Pt + SnO_2/C 30.70 III might be related to the efficient removal of CO poison from the Pt surface, which can be verified from the ratio between forward and backward current density scan peaks (j_f/j_b) [8,38]. Low j_f/j_b values indicate excessive amount of carbonaceous species adsorbed on catalyst surface, while higher ratios suggests less residues accumu-

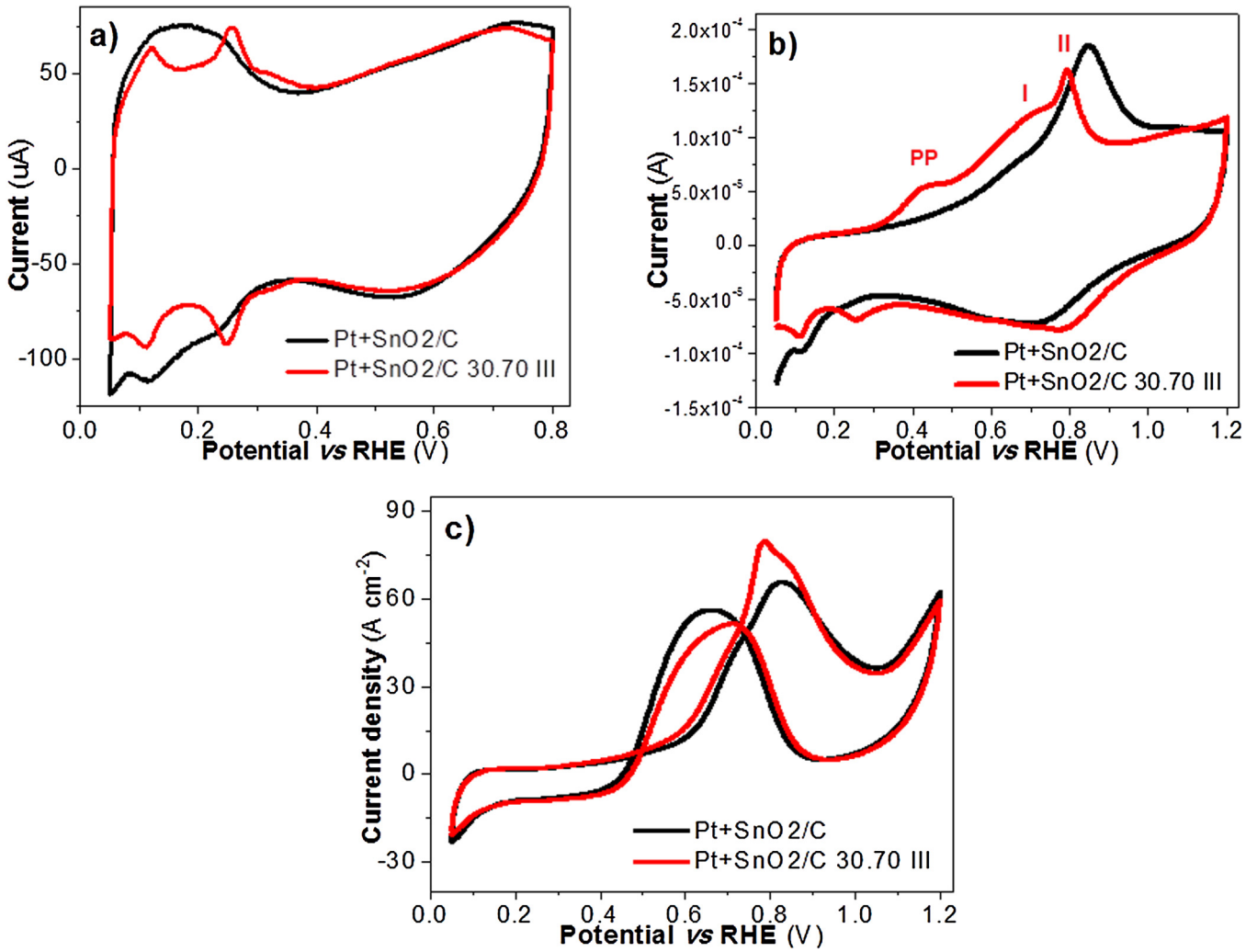

Fig. 4. Electrochemical tests **a)** CV profiles carried out into 0.5 mol L^{-1} of H_2SO_4 at 50 mV s^{-1}, **b)** CO-stripping technique recorded with a scan rate of 10 mV s^{-1} and **c)** CV with ethanol recorded with a scan rate of 10 mV s^{-1}.

lations, thus enhancing the catalytic response. The calculated j_f/j_b ratios were 1.56 for Pt + SnO_2/C 30.70 III and 1.15 for Pt + SnO_2/C. The latter value indicates that some EOR intermediates generated in forward scan were oxidized during the backward sweep. In Pt + SnO_2/C 30.70 III, however, the higher j_f/j_b value suggests that minor quantities of intermediates were produced during the forward sweep; consequently a greater amount of CO_2 was readily formed. Accordingly, it was found that oriented (100) Pt/C exhibited higher j_f/j_b values towards ethanol electro-oxidation than polycrystalline Pt/C [8]. Besides, there are other studies [20,23] revealing the effectiveness of Pt(100) in breaking the C—C bond, which is an obligatory step to CO_2 formation. In this sense, based on higher forward current density peak and j_f/j_b ratio, and the lower onset potential towards EOR, we can suggest that Pt + SnO_2/C 30.70 III not only may favor the break of C—C bond, but also lead to an easier CO oxidation compared to Pt + SnO_2/C, as seen in CO-stripping experiments. Indeed, it is desirable that all these benefits should be reproduced in fuel cell conditions since the results were performed in EOR separately.

Polarization and power density curves were chosen to evaluate the real electrical performance of the electrocatalysts, both normalized per cell electrode geometric area (5 cm^2). DEFC experiments were performed with MEAs containing both the prepared materials in anode side and commercial Pt/C in the cathodic side. From Fig. 5**a**, it can be observed the Pt + SnO_2/C 30.70 III open-circuit potential (OCP) was higher (~800 mV) than Pt + SnO_2/C (~760 mV), as well as its maximum current density (0.28 against 0.26 A cm^{-2}). The higher OCP and current densities at upper cell potential values of Pt + SnO_2/C 30.70 III could be related to the surface enhancement characteristics of Pt(100) in cleavage the C—C at such potentials, which can involve CO oxidation. Similar results were reported by Figueiredo et al. [20]. The lower electrical performance of Pt + SnO_2/C provided 47 mW cm^{-2}, while Pt + SnO_2/C 30.70 III supplied 58 mW cm^{-2} of maximum power density. Also, such maximum power density values achieved by Pt + SnO_2/C catalysts show the importance of the Pt + SnO_2 combination. For Pt/C catalyst, prepared by the same methodology but in absence of $SnCl_2$ and KBr (detailed in [24]), the maximum power density was almost 4.5 times lower (only 13 mW cm^{-2}) than for Pt + SnO_2/C 30.70 III. This result clearly demonstrates the improvement of SnO_2 composite on the overall device performance. The DEFC electrical performance is a result of ethanol electro-oxidation on anode side, forming acetaldehyde, acetic acid, ethyl acetate and CO_2. Ethyl acetate is formed from esterification reaction between ethanol and acetic acid; therefore its contribution was included in products quantification. Some anodic effluent aliquots were collected at a maximum current density condition, i.e., under cell potential close to zero, since all products concentration is higher at this condition. Based on the sum of unreacted ethanol and all products formed, the calculated mass balances were upper to 96% from the ethanol

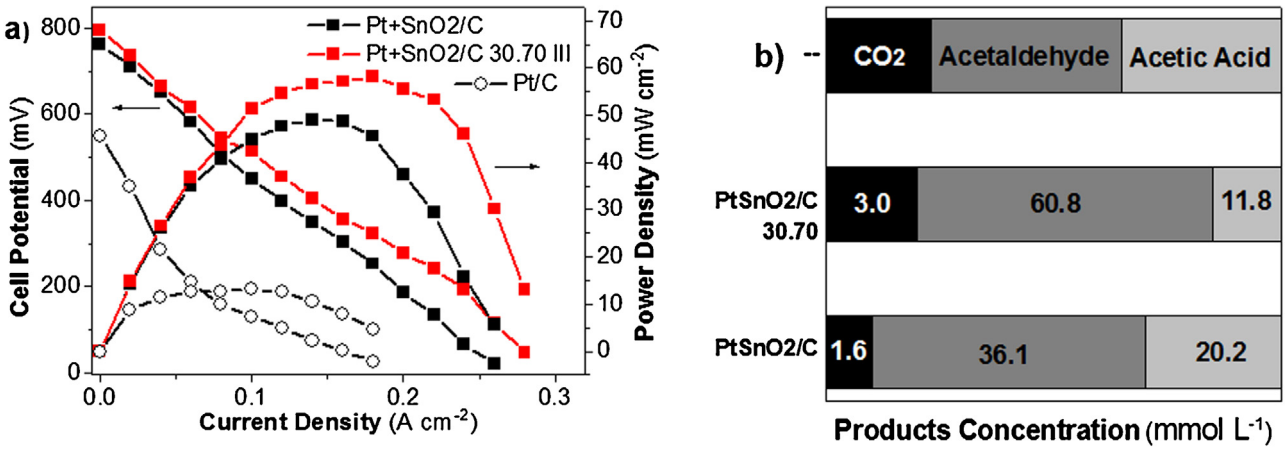

Fig. 5. **a)** Polarization and power density curves and **b)** products distribution analyzed by GC.

solution fuel, which are good values, considering the possibility of fuel crossover from anode to cathode. As it can be observed in Fig. 5**b**, the formed products (CO_2, acetaldehyde and acetic acid) correspond to a small percentage of ethanol fuel solution (ca. 4%) in this cell operation condition. No detectable CO_2 quantities by GC were observed at maximum power density condition for Pt/C [24]. This fact may suggest that such Pt active sites are fragile to CO poisoning, thus preventing the carbon dioxide formation and hence compromising the catalytic turnover. In relation to Pt, SnO_2 species can facilitate the activation of –OH necessary to oxidize CO (and other poisoning fragments) in CO_2, so the bifunctional effect of Pt + SnO_2 combination leads to a resultant enhancement on the DEFC electrical performance. The highest power density achieved by Pt + SnO_2/C 30.70 III can be understood through its increased reacted ethanol fuel into products quantity, which was in molar units approximately 30% higher than Pt + SnO_2/C and almost 64% higher than Pt/C [24]. Different products selectivity was found for both materials, yielding different number of involved electrons towards the ethanol electro-oxidation reaction. Despite the fact that CO_2 was produced in small quantities, its concentration yielded by Pt + SnO_2/C 30.70 III was almost double that formed by Pt + SnO_2/C, evidencing the ability of Pt(100) sites in oxidizing ethanol molecule completely. In both cases, acetaldehyde was produced in major quantities, 60.8 mmol L^{-1} for Pt + SnO_2/C 30.70 III and 36.1 mmol L^{-1} for Pt + SnO_2/C, while acetic acid was formed with 11.8 and 20.2 mmol L^{-1}, respectively. Different product amounts were attributed to their structure modifications, enhancing the cell electrical performance.

DEFC potential stability at constant current (0.5 A – equivalent value close at the maximum power density) was monitored fuelling with continuous ethanol solution during 90 min (Fig. 6**a**). It was observed two drops in both cell potentials, a rapid and notable

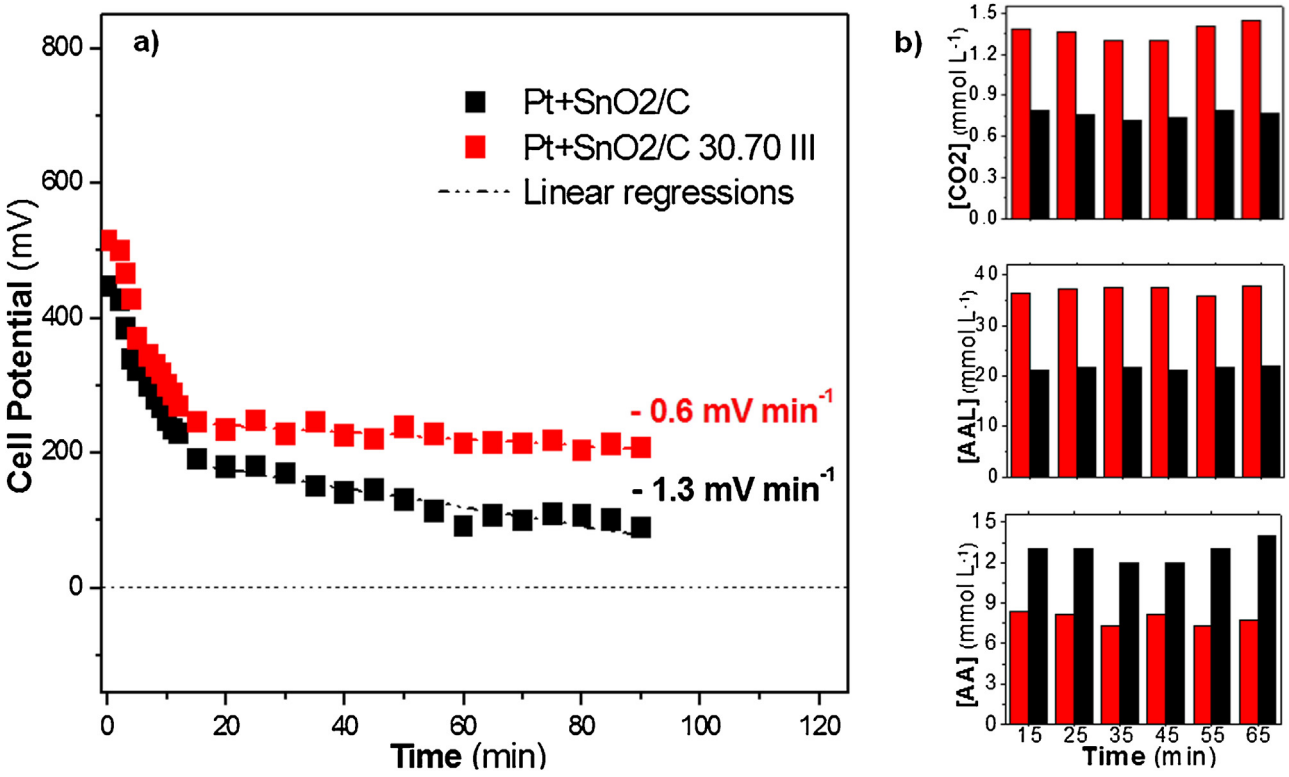

Fig. 6. **a)** Cell potential stability at 0.5 A with time and **b)** products analyses by GC.

deactivation during the first 15 min of DEFC operation, and after this period, a small potential decreased until the end of the test (slow deactivation). The cell potential decays with time until it attains a pseudo-steady state value. Such behavior resembles a chronoamperometric curve. The potential decay in the first situation could be attributed to the increasing accumulation of CO and other species (intermediaries from ethanol electro-oxidation) that hinder Pt active sites. In this stage, CO species (and others) concentration increase, hindering part of ethanol adsorption. The pseudo-steady state takes place when CO (and others intermediary species) accumulation attains a limit. In this second stage, cell potential continues to drop but in a mild way, suggesting intermediaries could also continue adsorbing on Pt sites. A linear regression was used to estimate the temporal cell potential drop ratio in the pseudo-steady state region. It was observed that both materials did not completely deactivate past 90 min of test. Pt + SnO_2/C exhibited less stability with a potential drop ratio of – 1.3 mV min^{-1}. Meanwhile, Pt + SnO_2/C 30.70 III showed not only higher potential values but also a greater stability of – 0.6 mV min^{-1}, indicating its higher efficiency to release the Pt active sites from adsorbed poisoning species.

The three products concentrations were reported during the test (Fig. 6**b**) and it is possible to note a similar distribution compared to the products analyzed in maximum current density condition. CO_2 and acetaldehyde quantities were approximately twice bigger for Pt + SnO_2/C 30.70 III while Pt + SnO_2/C yielded more acetic acid. In a previous work [25], we reported that Pt + SnO_2/C led a high selectivity to acetic acid formation compared to Pt/C. Herein, we also noted high acetic acid selectivity for Pt + SnO_2/C, but in Pt + SnO_2/C 30.70 III case, greater amounts of acetaldehyde and CO_2 were yielded. It is important to say that acetic acid practically cannot be further oxidized in DEFC operational conditions, but acetaldehyde can still be oxidized in CO_2 or acetic acid, releasing more electrons to the system [25].

This work clearly revealed the importance of nanoparticles morphology of Pt + SnO_2/C on ethanol electro-oxidation reaction and in DEFC electrical performance. We are now dedicating efforts to produce Pt + SnO_2/C electrocatalyst with cubic Pt (100) nanoparticles smaller than 5 nm in order to enhance the active surface per volume ratio.

4. Conclusion

In this report we successfully prepared Pt + SnO_2/C electrocatalyst containing nanoparticles with preferential Pt(100) orientation directly supported on carbon using only KBr as a shape directing agent. The order of addition of KBr, Pt and Sn precursors were important parameters in the reaction synthesis. Cubic Pt nanoparticles exposing Pt(100) facets with SnO_2 phase supported on carbon were exclusively achieved if Sn precursor is added when cubic Pt(100) nanoparticles were already formed, and after its addition, the reaction must not continue for a long time. X-ray diffractograms showed a decreased of (111)/(200) peak intensity ratio compared to Pt + SnO_2/C without KBr and cyclic voltammetry and CO-stripping experiments also indicated higher contents of Pt(100) exposed facets for cubic Pt + SnO_2/C electrocatalyst. Electrochemical experiments and DEFC tests showed that Pt + SnO_2/C containing Pt nanoparticles with Pt(100) preferential orientation was more active and selective to CO_2 than Pt + SnO_2/C polycrystalline electrocatalyst.

Acknowledgments

The authors thanks CNPq Proc. no 310051/2012-6, 443046/2014-0, 304869/2016-3 and FAPESP Proc. no 2014/09087-4 and CAPES for financial support. Use of TEM facilities (JEOL JEM-2100F) of LNNano-CNPEM is greatly acknowledged.

References

[1] S. Basri, S.K. Kamarudin, W.R.W. Daud, Z. Yaakub, Nanocatalyst for direct methanol fuel cell (DMFC), Int. J. Hydrogen Energy 35 (2010) 7957–7970.
[2] E. Antolini, Catalysts for direct ethanol fuel cells, J. Power Sources 170 (2007) 1–12.
[3] S. Song, P. Tsiakaras, Recent progress in direct ethanol proton exchange membrane fuel cells (DE-PEMFCs), Appl. Catal. B: Environ. 63 (2006) 187–193.
[4] A. Rouxoux, J. Schulz, H. Patin, Reduced transition metal colloids: a novel family of reusable catalysts, Chem. Rev. 102 (2002) 3757–3778.
[5] W. Lu, B.-X. Mi, M.C.W. Chan, H. Zheng, C.-M. Che, N. Zhu, S.-T. Lee, Light-emitting tridentate CyclometalatedPlatinum(II) complexes containing (-alkynyl auxiliaries: Tuning of photo- and electrophosphorescence, J. Am. Chem. Soc. 126 (2004) 4958–4971.
[6] R. Polsky, R. Gill, L. Kaganovsky, I. Willner, Nucleic acid-functionalized Pt nanoparticles: catalytic labels for the amplified electrochemical detection of biomolecules, Anal. Chem. 78 (2006) 2268–2271.
[7] S. Guo, E. Wang, Noble metal nanomaterials: controllable synthesis and application in fuel cells and analytical sensors, Nano Today 6 (2011) 240–264.
[8] S.-B. Han, Y.-J. Song, J.-M. Lee, J.-Y. Kim, K.-W. Park, Platinum nanocube catalysts for methanol and ethanol electrooxidation, Electrochem. Commun. 10 (2008) 1044–1047.
[9] J. Zhang, W. Yao, M. Liu, Q. Xu, Q. Wu, T. Zeng, Shape controlled synthesis of platinum nanocrystals with high catalytic activities for methanol electrooxidation, Catal. Lett. 143 (2013) 1030–1034.
[10] T.S. Ahmadi, Z.L. Wang, A. Henglein, M.A. El-Sayed, Cubic colloidal platinum nanoparticles, Chem. Mater. 8 (1996) 1161–1163.
[11] K.S. Napolskii, P.J. Barczuk, S.Y. Vassiliev, A.G. Veresov, G.A. Tsirlina, P.J. Kulesza, Templating of electrodeposited platinum group metals as a tool to control catalytic activity, ElectrochimicaActa 52 (2007) 7910–7919.
[12] K. Miyabayashi, S. Nakamura, M. Miyake, Synthesis of small platinum cube with less than 3 nm by the control of growth kinetics, Cryst. Growth Des. 11 (2011) 4292–4295.
[13] X. Gong, Y. Yang, L. Zhang, C. Zou, P. Cai, G. Chen, S. Huang, Controlled synthesis of Pt nanoparticles via seeding growth and their shape-dependent catalytic activity, J. Colloid Interface Sci. 352 (2010) 379–385.
[14] H. Song, R.M. Rioux, J.D. Hoefelmeyer, R. Komor, K. Niesz, M. Grass, P. Yang, G. ASomorjai, Hydrothermal growth of mesporous SBA-15 silica in the presence of PVP-stabilized Pt nanoparticles: synthesis, characterization, and catalytic properties, J. Am. Chem. Soc. 128 (2006) 3027–3037.
[15] D. Li, C. Wang, D. Tripkovic, S. Sun, N.M. Markovic, V.R. Stamenkovic, Surfactant removal for colloidal nanoparticles from solution synthesis: the effect on catalytic performance, ACS Catal. 2 (2012) 1358–1362.
[16] J. Monzó, M.T.M. Koper, P. Rodriguez, Removing polyvinylpyrrolidone from catalytic Pt nanoparticles without modification of superficial order, ChemPhysChem 13 (2012) 709–715.
[17] J.M. Krier, W.D. Michalak, L.R. Baker, K. An, K. Komvopoulos, G.A. Somorjai, Sum frequency generation vibrational spectroscopy of colloidal platinum nanoparticle catalysts: disordering versus removal of organic capping, J. Phys. Chem. C 116 (2012) 17540–17546.
[18] J.A. Michel, W.H. Morris, C.M. Lukehart, Synthesis of shaped Pt nanoparticles using common anions or small molecules as shape-directing agents: observation of a strong halide or pseudo-halide effect, J. Mater. Chem. A 5 (2015) 2012–2018.
[19] C. Kim, S.S. Kim, S. Yang, J.W. Han, H. Lee, In situ shaping of Pt nanoparticles directly overgrown on carbon supports, Chem. Commun. 48 (2012) 6396–6398.
[20] M.C. Figueiredo, J. Solla-Gullón, F.J. Vidal-Iglesias, M. Nisula, J.M. Feliu, T. Kallio, Carbon-supported shape-controlled Pt nanoparticle electrocatalysts for direct alcohol fuel cells, Electrochem. Commun. 55 (2015) 47–50.
[21] R.A. Martınez-Rodríguez, F.J. Vidal-Iglesias, J. Solla-Gullon, C.R. Cabrera, J.M. Feliu, Synthesis of Pt nanoparticles in water-in-oil microemulsion: effect of HCl on their surface structure, J. Am. Chem. Soc. 136 (2014) 1280–1283.
[22] F.J. Vidal-Iglesias, V. Montiel, J. Solla-Gullón, Influence of the metal loading on the electrocatalytic activity of carbon-supported (100) Pt nanoparticles, J. Solid State Electrochem. 20 (2016) 1107–1118.
[23] C. Busó-Rogero, V. Grozovski, F.J. Vidal-Iglesias, J. Solla-Gullón, E. Herrero, J.M. Feliu, Surface structure and anion effects in the oxidation of ethanol on platinum nanoparticles, J. Mater. Chem. A 1 (2013) 7068–7076.
[24] R.M. Antoniassi, L. Otubo, J.M. Vaz, A. Oliveira Neto, E.V. Spinacé, Synthesis of Pt nanoparticles with preferential (100) orientation directly on the carbon support for direct ethanol fuel cell, J. Catal. 342 (2016) 67–74.
[25] R.M. Antoniassi, A. Oliveira Neto, M. Linardi, E.V. Spinace, The effect of acetaldehyde and acetic acid on the direct ethanol fuel cell performance using PtSnO2/C electrocatalysts, Int. J. Hydrogen Energy 38 (2013) 12069–12077.
[26] L. Jiang, G. Sun, Z. Zhou, S. Sun, Q. Wang, S. Yan, H. Li, J. Tian, J. Guo, B. Zhou, Q. Xin, Size-controllable synthesis of monodispersed SnO_2 nanoparticles and application in electrocatalysts, J. Phys. Chem. B 109 (2005) 8774–8778.
[27] V.P. dos Santos, G. Tremiliosi Filho, Correlação entre a Estrutura Atômica Superficial e o Processo de Adsorção-Dessorção Reversível de Hidrogênio em Eletrodos MonocristalinosPt(111), Pt(100) e Pt(110) Quim, Nova 24 (2001) 856–863.

[28] F.J. Vidal-Iglesias, R.M. Arán-Ais, J. Solla-Gullón, E. Herrero, J.M. Feliu, Electrochemical characterization of shape-controlled Pt nanoparticles in different supporting electrolytes, ACS Catal. 2 (2012) 901–910.
[29] C.C. Caliman, L.M. Palma, J. Ribeiro, Evaluation of Ni and Ti addition in PtSn/C catalysts for ethanol and glycerol electrooxidation, J. Electrochem. Soc. 160 (2013) 853–858.
[30] D. WANG, J. WANG, S. LU, S.P. JIANG, Facile synthesis of sub-monolayer Sn, Ru, and RuSn decorated Pt/C nanoparticles for formaldehyde electrooxidation, J. Electroanal. Chem. 172 (2014) 55–61.
[31] Y. Chen, J. Shi, S. Chen, Small-molecule (CO, H2) electro-oxidation as an electrochemical tool for characterization of Ni@Pt/C with different Pt coverages, J. Phys. Chem. C 119 (2015) 7138–7145.
[32] M. Zhu, G. Sun, H. Li, Q. Cao, Effect of the Sn(II)/Sn(IV) redox couple on the activity of PtSn/C for ethanol electro-oxidation, Chinese J. Catal. 29 (2008) 765–770.
[33] D. Lee, S. Hwang, I. Lee, A study on composite PtRu(1:1)-PtSn(3:1) anode catalyst for PEMFC, J. Power Sources 145 (2005) 147–153.
[34] Y. Ye, J. Joo, S. Lee, J. Lee, A direct one-step synthetic route to Pd-Pt nanostructures with controllable shape, size, and composition for electrocatalytic applications, J. Mater. Chem. A 2 (2014) 19239–19246.
[35] P. Urchaga, S. Baranton, C. Coutanceau, Changes in COchem oxidative stripping activity induced by reconstruction of Pt (111) and (100) surface nanodomains, ElectrochimicaActa 92 (2013) 438–445.
[36] S. Brimaud, S. Pronier, C. Coutanceau, J.-M. Léger, New findings on CO electrooxidation at platinum nanoparticle surfaces, Electrochem. Commun. 10 (2008) 1703–1707.
[37] C. Coutanceau, P. Urchaga, S. Baranton, Diffusion of adsorbed CO on platinum (100) and (111) oriented nanosurfaces, Electrochem. Commun. 22 (2012) 109–112.
[38] Z. Liu, L. Hong, Electrochemical characterization of the electrooxidation of methanol, ethanol and formic acid on Pt/C and PtRu/C electrodes, J. Appl. Electrochem. 37 (2007) 505–510.